

Fast and Accurate Multi-Body Simulation with Stiff Viscoelastic Contacts

Bilal Hammoud¹, Luca Olivieri², Ludovic Righetti¹, Justin Carpentier³, Andrea Del Prete²

Abstract—The simulation of multi-body systems with frictional contacts is a fundamental tool for many fields, such as robotics, computer graphics, and mechanics. Hard frictional contacts are particularly troublesome to simulate because they make the differential equations stiff, calling for computationally demanding implicit integration schemes. We suggest to tackle this issue by using exponential integrators, a long-standing class of integration schemes (first introduced in the 60’s) that in recent years has enjoyed a resurgence of interest. We show that this scheme can be easily applied to multi-body systems subject to stiff viscoelastic contacts, producing accurate results at lower computational cost than classic explicit schemes. In our tests with quadruped and biped robots, our method demonstrated stable behaviors with large time steps (10 ms) and stiff contacts (10^5 N/m). Its excellent properties, especially for fast and coarse simulations, make it a valuable candidate for many applications in robotics, such as simulation, Model Predictive Control, Reinforcement Learning, and controller design.

I. INTRODUCTION

The interest of the robotics community for fast and reliable methods to simulate multi-body systems subject to frictional contacts has been constantly growing in the last two decades [1], [2], [3], [4], [5]. This is reasonable considering that simulation is at the core of many robotics applications, such as the development and testing of novel controllers before deployment on hardware. Moreover, many advanced control and planning techniques (Model Predictive Control [6], and Optimal Control) rely on the ability to predict the future behavior of the system. Finally, the current bottleneck of many learning algorithms [7], [8] is their need for huge amounts of data, which therefore can greatly benefit from fast and accurate simulation methods.

The simulation of multi-body systems without contacts is a solved problem [9]. The same is not the case for systems with stiff contacts, which can be treated in two ways, each leading to a hard (but different) numerical problem. The first approach, which more closely follows the physical phenomenon of contacts, consists in expressing contact forces as a function of the penetration between bodies. Often, linear spring dampers have been used in this context [5], [10]. This leads to stiff differential equations that are simple to evaluate, but difficult to integrate because of their *numerical stiffness* [11]. The second approach tries to circumvent these numerical challenges by assuming contacts to be *infinitely*

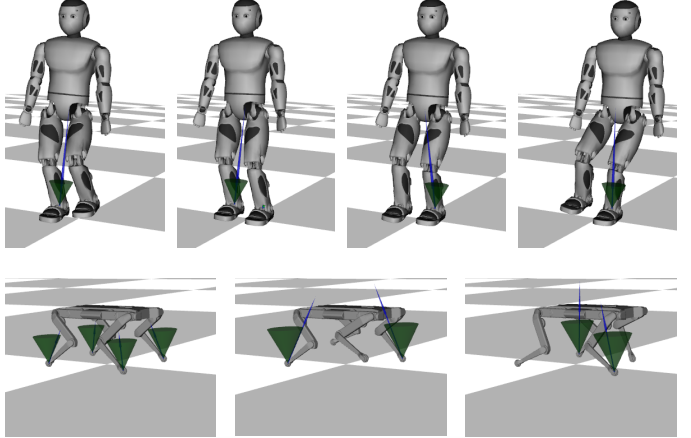


Fig. 1: Snapshots from our simulation tests with a biped and a quadruped robot.

rigid. This approach effectively gets rid of the numerical stiffness, but in exchange for *non-smoothness*. One method that has been particularly successful for dealing with the resulting non-smooth equations is velocity-impulse time-stepping [12], [1], [4]. This has become the standard for robot simulation [13], demonstrating stable behaviors with large time steps (several ms)—even though it must solve a numerically hard Linear Complementarity Problem (LCP). Several authors have tried to improve this approach by getting rid of the strict complementarity constraints [2], [14], [3], which are the source of the numerical challenge. However, none of these approaches is currently widely accepted in the robotics community, mainly because of the unclear effects of the introduced numerical regularization/relaxations in terms of physics.

The approach we advocate for in this paper is based on a well-known soft contact model: the linear spring damper. Instead of using explicit integration schemes, which require small time steps, or implicit schemes, which require solving nonlinear systems of equations and introduce artificial viscosity leading to nonphysical behaviors, we use *Exponential Integrators* (EI) [15]. EI are a long-standing class of integration schemes [16] that are particularly suited for stiff differential equations. EI were initially considered unpractical because of the computational challenges related to the matrix exponential [17]. However, novel numerical methods to compute the matrix exponential [18], [19], [20] have recently unlocked the potential of EI. This has already been used in computer graphics for simulating deformable

¹Tandon School of Engineering, New York University, New York, USA. bilal.hammoud@nyu.edu, ludovic.righetti@nyu.edu

²Department of Industrial Engineering, University of Trento, Italy luca.olivieri-1@unitn.it, andrea.delprete@unitn.it

³INRIA, Paris, France justin.carpentier@inria.fr

objects, modeled as systems of particles [21], [22], [23]. This model is particularly suited for EI because the stiff part of the dynamics is linear, which however is not the case for articulated systems in contact with the environment.

Our main contribution is a simulation algorithm that exploits EI to simulate articulated robots in contact with a stiff visco-elastic environment. To do that in an efficient way, we apply EI only to the contact dynamics (which is stiff) while using an explicit Euler scheme for the remaining terms (which are not stiff). Our simulation results on quadruped and biped robots (see Fig. 1) show the superior performance of our method compared to explicit Euler and semi-implicit Euler in terms of accuracy, speed and stability. To our knowledge, this class of integrators has never been used before by the robotics community. The paper is organized as follows. Section II introduces the problem of multi-body simulation and the basic theory of EI. Section III explains how EI can be used for multi-body simulation with bilateral contacts. This method is then extended to frictional contacts in Section IV. Section V discusses the implementation details of the algorithm. Section VI presents the results and Section ?? concludes the paper.

II. BACKGROUND

A. Multi-Body Dynamics and Soft Contact Model

We want to simulate a multi-body mechanical system with the following dynamics [9]:

$$M(q)\dot{v} = u(q, v) + J(q)^\top \lambda, \quad (1)$$

where q is the robot joint configuration, v is the robot joint velocity, M is the joint space mass matrix, u contains gravity, nonlinear effects and actuator forces, J is the contact point Jacobian, and λ contains the stacked 3D contact forces. We assume a linear spring-damper contact model, which means that the contact forces λ are proportional to the interpenetration of contacting bodies:

$$\lambda = -K \underbrace{(p(q) - p_0)}_{\Delta p} - B \underbrace{(\dot{p}(q, v) - \dot{p}_0)}_{\Delta \dot{p}}, \quad (2)$$

where p and \dot{p} contain the stacked 3D contact point positions and velocities, p_0 and \dot{p}_0 contain the stacked 3D anchor point positions and velocities, and K and B are the diagonal stiffness and damping matrices, respectively. The anchor point p_0 is a *virtual* point to which the *virtual* spring and damper are attached. It is typically set to the contact point location when contact is first detected, and as long as contacts are sticking $\dot{p}_0 = 0$. However, when slipping occurs then $\dot{p}_0 \neq 0$. Dependencies on q and v are dropped in the following to ease notation.

B. Explicit Integration Schemes

The classic approach to integrate this dynamical system starts by writing it in standard form. Defining the state as $x_q \triangleq (q, v)$, its dynamics is:

$$\underbrace{\frac{d}{dt} \begin{bmatrix} q \\ v \end{bmatrix}}_{\dot{x}_q} = \underbrace{\begin{bmatrix} v \\ M^{-1}(u + J^\top \lambda) \end{bmatrix}}_{f(x_q, u)} \quad (3)$$

We can integrate (3) with any numerical integration scheme, such as a high-order Runge-Kutta scheme, or even a simple explicit Euler [11] (very common in robotics):

$$x_q^+ = x_q + \delta t f(x_q, u) \quad (4)$$

where x_q^+ represents the next value of the state and δt is the integration time step. The problem with this approach is that for large values of K and B the differential equations (3) are *stiff* [11]. This means that they require very small integration steps for numerical stability. This is the main reason why soft contact models have been mostly abandoned in the last decade, in favor of complementarity-based models (and their relaxations) and time-stepping integration schemes [2], [24], [4].

C. Exponential Integrators (EI)

EI [22], [23], [21] are integration schemes particularly suited for stiff dynamical systems for which the *stiffness* comes from a linear part of their dynamics:

$$\dot{x} = \underbrace{f(x)}_{\text{nonstiff nonlinear function}} + \underbrace{Ax}_{\text{stiff linear function}} \quad (5)$$

In this case, using an explicit integration scheme would result in the problems mentioned above. Instead, EI exploit the linearity of the stiff part of the dynamics, which can be solved *analytically* using the matrix exponential, thanks to the well-known solution of linear dynamical systems:

$$\begin{aligned} \dot{x}(t) &= Ax(t) + b \\ x(t) &= e^{tA}x(0) + \int_0^t e^{\tau A} d\tau b \end{aligned} \quad (6)$$

First-order EI apply the solution (6) to the nonlinear system (5), by interpreting $f()$ as b and assuming it remains constant during the integration step:

$$x(t) = e^{tA}x(0) + \int_0^t e^{\tau A} d\tau f(x(0)) \quad (7)$$

Since the stiff part of the equations is integrated via the matrix exponential, large integration steps can be taken, resulting in faster simulations.

III. BILATERAL CONTACTS

Our approach consists in using EI to simulate the system (3). This is not trivial because (3) does not appear in the form (5), which is needed by EI. The standard approach to apply EI to arbitrary dynamics is to use a 1-st order Taylor expansion:

$$\dot{x}_q(t_0 + t) \approx \dot{x}_q(t_0) + \frac{\partial f}{\partial x_q}(x_q(t_0 + t) - x_q(t_0)) \quad (8)$$

However this would require a time-consuming computation of the dynamics Jacobian, so we use a different approach.

To get a differential equation with the form (5) we start by projecting (1) in contact space pre-multiplying both sides by $J M^{-1}$:

$$J\dot{v} - \underbrace{J M^{-1} J^\top}_{\Upsilon} \lambda = \underbrace{J M^{-1} u}_{\dot{v}} \quad (9)$$

Then we use the relationship $\ddot{p} = J\dot{v} + \dot{J}v$ to express the contact point accelerations as functions of the robot accelerations:

$$\begin{aligned} \ddot{p} - \Upsilon\lambda &= J\dot{v} + \dot{J}v \\ \ddot{p} + \Upsilon K\Delta p + \Upsilon B\Delta\dot{p} &= \underbrace{J\dot{v} + \dot{J}v}_{\ddot{p}} \end{aligned} \quad (10)$$

Assuming $\ddot{p}_0 = 0$ (i.e. instantaneous anchor point velocity changes) we can write the contact point dynamics as:

$$\frac{d}{dt} \begin{bmatrix} \Delta p \\ \Delta \dot{p} \end{bmatrix} = \underbrace{\begin{bmatrix} 0 & I \\ -\Upsilon K & -\Upsilon B \end{bmatrix}}_A \underbrace{\begin{bmatrix} \Delta p \\ \Delta \dot{p} \end{bmatrix}}_x + \underbrace{\begin{bmatrix} 0 \\ \ddot{p} \end{bmatrix}}_b \quad (11)$$

This dynamical system does not have the same form as (5) because Υ (and thus A) depends on q . However, Υ is typically a well-conditioned function, meaning that it changes little for small variations of q . The same holds for \ddot{p} (and thus b), which is why multi-body systems without contacts can typically be integrated with large time steps (≈ 5 ms). This means that we can approximate A and b as constants during the integration step, and therefore treat (11) as linear. We can now express the contact forces as:

$$\lambda(t) = \underbrace{\begin{bmatrix} -K & -B \end{bmatrix}}_D x(t) = D e^{tA} x(0) + D \int_0^t e^{\tau A} d\tau b \quad (12)$$

Substituting (12) in (3) we can compute the robot accelerations:

$$\dot{v}(t) = M^{-1}(u + J^\top \lambda(t)) = \dot{\bar{v}} + M^{-1} J^\top D x(t), \quad (13)$$

where we consider all terms constant during the integration step, except for $x(t)$. Now we can integrate to get the new velocities v^+ :

$$\begin{aligned} v^+ &= v + \int_0^{\delta t} \dot{v}(\tau) d\tau = \\ &= v + \delta t \dot{\bar{v}} + M^{-1} J^\top D \int_0^{\delta t} x(\tau) d\tau \end{aligned} \quad (14)$$

Finally we integrate twice to get the new configuration q^+ :

$$\begin{aligned} q^+ &= q + \int_0^{\delta t} v(\tau) d\tau = \\ &= q + \delta t v + \frac{\delta t^2}{2} \dot{\bar{v}} + M^{-1} J^\top D \int_0^{\delta t} \int_0^\tau x(\tau_1) d\tau_1 d\tau \end{aligned} \quad (15)$$

A. Integration of Matrix Exponentials

Eq. (14) and (15) are straightforward to compute, except for their last terms, which are:

$$\begin{aligned} x_{int}(t) &\triangleq \int_0^t x(\tau) d\tau \\ x_{int2}(t) &\triangleq \int_0^t \int_0^\tau x(\tau_1) d\tau_1 d\tau, \end{aligned} \quad (16)$$

where

$$x(t) = e^{tA} x(0) + \int_0^t e^{\tau A} d\tau b \quad (17)$$

When A is invertible we can express the integral of e^{tA} as an algebraic function of e^{tA} :

$$\int_0^t e^{\tau A} d\tau = A^{-1}(e^{tA} - I) \quad (18)$$

However, A is not invertible if the contact Jacobian J is not full-row rank. Luckily, the computation of integrals involving matrix exponentials has been thoroughly investigated [25], [26]. In Section V we show how to compute these integrals indirectly, by simply computing the matrix exponentials of an augmented system.

B. Extension to non-Euclidian spaces

When q does not belong to an Euclidian space (as in the case of legged robots) the integration of q is slightly more complicated (while the integration of v remains unchanged). Given the following definition:

$$v_{mean} \triangleq v + \frac{\delta t}{2} \dot{\bar{v}} + \frac{1}{\delta t} M^{-1} J^\top D x_{int2}(\delta t) \quad (19)$$

The integration step of q is computed as:

$$q^+ = \text{integrate}(q, \delta t v_{mean}), \quad (20)$$

where the function $\text{integrate}(\cdot)$ performs integration in the non-Euclidian space of q .

IV. FRICTIONAL CONTACTS

So far we have assumed that contact forces were bilateral. However, we typically want to simulate unilateral contacts, where forces oppose penetration but do not oppose detachment of bodies. Assuming that the contact forces are expressed in a local reference frame with the z direction aligned with the contact normal, unilateral forces must satisfy:

$$f_i^z \geq 0 \quad \forall i \quad (21)$$

Moreover, tangential forces are typically limited as well. Assuming a Coulomb friction model we have:

$$\sqrt{(f_i^x)^2 + (f_i^y)^2} \leq \mu f_i^z \quad \forall i, \quad (22)$$

where $\mu \in \mathbb{R}^+$ is the coefficient of friction. We can represent the constraints (21) and (22) as $\lambda \in \mathcal{K}_\mu$, with \mathcal{K}_μ being a second-order cone.

A. Force Projection

To account for these constraints, when the value of $\lambda(t)$ computed by (12) is outside \mathcal{K}_μ , we should project it on the boundaries of \mathcal{K}_μ . However, we do not know how to check this constraint in continuous time. In the same spirit of time-stepping simulators [1], we suggest to check friction constraints on the average value of $\lambda(t)$ during the integration step, which is:

$$\bar{\lambda} \triangleq \frac{1}{\delta t} \int_0^{\delta t} \lambda(\tau) d\tau = \frac{1}{\delta t} D x_{int}(\delta t) \quad (23)$$

If $\bar{\lambda} \notin \mathcal{K}_\mu$, then we compute its projection on the boundaries of the friction cone $\lambda_{pr} = \text{proj}_{\mathcal{K}_\mu}(\bar{\lambda})$ and we use it to compute the next state:

$$\begin{aligned}\dot{v}_{pr} &\triangleq M^{-1}(u + J^\top \lambda_{pr}) \\ v^+ &= v + \delta t \dot{v}_{pr} \\ q^+ &= q + \delta t v + \frac{\delta t^2}{2} \dot{v}_{pr}\end{aligned}\quad (24)$$

Note that in case $\bar{\lambda} \in \mathcal{K}_\mu$, then $\lambda_{pr} = \bar{\lambda}$ and the velocity update in (24) is equivalent to (14). However, the position update in (24) approximates the double integral of $\lambda(t)$ assuming a constant force (λ_{pr}), and so it is not equivalent to (15) in general. In order to exploit also the double integral of $x(t)$, we can check the friction cone constraints on the average of the average $\lambda(t)$, computed as:

$$\bar{\lambda} \triangleq \frac{2}{\delta t^2} \int_0^{\delta t} \int_0^\tau \lambda(\tau_1) d\tau_1 d\tau = \frac{2}{\delta t^2} D x_{int2}(\delta t) \quad (25)$$

If $\bar{\lambda} \notin \mathcal{K}_\mu$, then we project it on the boundaries of the friction cone $\lambda_{pr2} = \text{proj}_{\mathcal{K}_\mu}(\bar{\lambda})$ and we use it to compute the next position:

$$\begin{aligned}\dot{v}_{pr2} &\triangleq M^{-1}(u + J^\top \lambda_{pr2}) \\ q^+ &= q + \delta t v + \frac{\delta t^2}{2} \dot{v}_{pr2}\end{aligned}\quad (26)$$

Using (26) for the position update and (24) for the velocity update, both updates are equivalent to the original ones in case of no slippage.

B. Anchor point update

When slippage occurs, the tangent anchor point state (p_0^t, p_0^t) (where the index t indicates the tangent directions) should be updated so that the contact forces at the end of the time step are inside the friction cones. When a contact starts slipping, the tangent anchor point velocity quickly converges to \dot{p}^t . We neglect the transient and as soon as slippage starts we set $\dot{p}_0^t := \dot{p}^t$. Then, we compute p_0^t so that the contact force is on the boundary of the friction cone:

$$\begin{aligned}\lambda &:= \text{proj}_{\mathcal{K}_\mu}(\lambda) \\ p_0^t &:= p^t + (K^t)^{-1} \lambda^t\end{aligned}\quad (27)$$

V. COMPUTATIONAL ASPECTS

The computational bottleneck of the presented approach is the computation of x_{int} and x_{int2} defined in (16). This section shows how to compute these quantities with a matrix exponential, and how this computation can be sped up.

A. Computing x_{int} and x_{int2}

Using the results presented in [26] we can compute x_{int} and x_{int2} as:

$$[x_{int}(t) \quad x_{int2}(t)] = [I_n \quad 0_{n \times 3}] e^{t\bar{A}} \begin{bmatrix} 0_{(n+1) \times 2} \\ I_2 \end{bmatrix} \quad (28)$$

where \bar{A} is an augmented matrix slightly larger than A :

$$\bar{A} \triangleq \begin{bmatrix} A & b & x(0) & 0 \\ 0 & 0 & 1 & 0 \\ 0 & 0 & 0 & 1 \\ 0 & 0 & 0 & 0 \end{bmatrix} \quad (29)$$

B. Computing the Matrix Exponential

Using (28) we have transformed the problem of computing (16) into a matrix exponential evaluation. Computing the matrix exponential is a challenging but well-understood numerical problem [18], [27], [19], [20]. We have used as starting point the scaling&squaring method, as revisited by Higham [18], a widely used method for computing the exponential of small-medium size dense matrices. The method scales the matrix by a power of 2 to reduce the norm to order 1, computes a Padé approximant to the matrix exponential, and then repeatedly squares to undo the effect of the scaling. A Padé approximant of a function is its “best” approximation achievable by a ratio of two polynomials $D_j(\cdot)$, $N_j(\cdot)$ of order j :

$$e^A \approx D_j(A)^{-1} N_j(A) \quad (30)$$

These approximants are only accurate around zero, so they cannot be used directly if $\|A\|$ is large. When that is the case, the scaling&squaring method is used to reduce $\|A\|$ by exploiting this property of the exponential:

$$e^A = (e^{A/(2^s)})^{2^s} \quad (31)$$

The integer scaling parameter s is chosen so that $\|e^{A/(2^s)}\|$ is sufficiently small.

C. Boosting the Matrix Exponential Computation

Our problem has two features that we can exploit to speed up computation:

- 1) We do not need double machine precision, i.e. $\approx 10^{-16}$, (which is the target of the algorithm of [18]) because we are typically fine with much larger numerical integration errors, e.g. $\approx 10^{-4}$.
- 2) We do not need the whole matrix exponential, but only its product with a 2-column matrix, as shown in (28).

The first point is easily exploitable. The choice of the scaling parameter s and the polynomial order j is usually optimized to achieve double machine precision with the minimum amount of matrix-matrix multiplications. We have empirically found that for our tests we can set $s = 0$ and use a relatively low order $j \in [1, 2, 3, 5, 7]$, corresponding to $[0, 1, 2, 3, 4]$ matrix-matrix multiplications, respectively. Which polynomial order is optimal depends on the specific test, and is discussed in the next section.

Regarding the second point, given a matrix V , we can directly compute the product $e^A V$ by performing operations in the following order:

$$\begin{aligned}V_1 &:= N_j(A) V \\ e^A V &:= D_j(A)^{-1} V_1\end{aligned}\quad (32)$$

This is faster than computing e^A and then multiplying it times V because we have to solve the linear system with a much smaller right-hand-side (V_1 rather than N_j).

Finally, we have also observed that the preprocessing step suggested in [18], which uses *matrix balancing*, is extremely effective at reducing $\|A\|$ in our tests. This is crucial to achieve accurate results with low polynomial

TABLE I: Controller time steps.

| Test | δt_c [ms] | Test | δt_c [ms] |
|------------|-------------------|------------|-------------------|
| Solo-squat | 10 | Solo-trot | 2 |
| Solo-jump | 10 | Romeo-walk | 40 |

orders, therefore speeding up computations. Further details on our implementation can be found in our open-source online repository¹.

VI. RESULTS

We assess the performance of our simulation algorithm (*Expo*) comparing it to explicit Euler (*Eul-exp*):

$$\begin{aligned} v^+ &= v + \delta t \dot{v} \\ q^+ &= \text{integrate}(q, \delta t v + \frac{\delta t^2}{2} \dot{v}), \end{aligned} \quad (33)$$

and to semi-implicit Euler (*Eul-semi*):

$$\begin{aligned} v^+ &= v + \delta t \dot{v} \\ q^+ &= \text{integrate}(q, \delta t v^+), \end{aligned} \quad (34)$$

Our results try to answer to the following questions:

- 1) Can our approach (compared to the others) achieve higher accuracy for equal computation time, or equal accuracy for smaller computation time? (Section VI-A)
- 2) How sensitive is the simulator accuracy to contact stiffness and damping? (Section VI-B)
- 3) What is the maximum integration time step that results in a stable motion? (Section VI-C)
- 4) How accurately can (11) predict future contact forces when assuming constant A and b ? (Section VI-D)
- 5) How much computation time is spent in the different operations of our simulator? (Section VI-E)

1) *Accuracy Metric*: Following an approach similar to [13], we measure accuracy with a *local integration error*. We compute the ground truth trajectory $x_q(t)$ using the simulator under analysis (either *Expo*, or *Eul-exp*, or *Eul-semi*) with an extremely small time step $\delta t = 1/64$ ms. Let us define $\hat{x}_q(t; t - \delta t_c, x_q(t - \delta t_c))$ as the state at time t obtained by numerical integration starting from the ground-truth state $x_q(t - \delta t_c)$, where $\delta t_c (\geq \delta t)$ is the time step of the controller. We define the *local* integration error as the error accumulated over one control time step:

$$e(t) \triangleq \|x_q(t) \ominus \hat{x}_q(t; t - \delta t_c, x_q(t - \delta t_c))\|_\infty$$

where \ominus is a difference operator on the space where x_q is defined. In the numerical integration literature [11] the *local* integration (or truncation) error is typically defined using the integration step δt rather than the controller step δt_c . We chose to use the controller step to make errors comparable across tests with different integration steps (as in [13]).

2) *Test Description*: To evaluate the trade-off between accuracy and computation time we tested each simulator with different time steps. For *Expo* we have started from $\delta t = 1/8$ ms up to the controller time step $\delta t = \delta t_c$ with a logarithmic

step of 2 (i.e. $1/8, 1/4, \dots, \delta t_c/2, \delta t_c$). For the other simulators we have used the same approach, but starting from a value of δt so as to get roughly the same computational speed as *Expo*. For every test we have set δt_c to the largest value that still ensured control stability (see Table I). Since our main interest lies in legged robots, our tests focused on quadrupeds and bipeds:

- *Solo-squat*: Quadruped robot Solo [28] performing a squatting motion.
- *Solo-jump*: Quadruped robot Solo jumping in place.
- *Solo-trot*: Quadruped robot Solo trotting forward.
- *Romeo-walk*: Humanoid robot Romeo [29] taking two walking steps.

If not specified otherwise, we have used a contact stiffness $K = 10^5$ N/m, and a contact damping $B = 300$ Ns/m, which are reasonable values for contacts with a hard floor. For homogeneity we have used the same value of friction coefficient $\mu = 1$ across all our tests, even though this large friction was only needed for control stability of the quadruped jumping motion. Besides testing the default *Expo* simulator, we also tested 5 other versions of the same scheme where we used a reduced polynomial order in the Padé approximant of the matrix exponential. This leads to a reduced number of matrix-matrix multiplications (mmm), between 0 and 4 (see Section V-C). This results in a faster but potentially less accurate computation of the matrix exponential.

All the code has been implemented in C++ and binded with Python. For all dynamics computation we have used the Pinocchio library [30].

A. Accuracy-Speed Results

Fig. 2 shows the results for the four tests, plotting *local errors* vs *real-time factor*, which measures how many times the simulation was faster than real time. Overall, *Expo* outperformed *Eul-exp* in all our tests, showing faster computation for equal accuracy, or greater accuracy for equal computation time. These results show a sudden increase of integration error of *Eul-exp* for large real-time factors—corresponding to large δt . This is because of the well-known poor stability of explicit Euler. Semi-implicit Euler performed almost the same as explicit Euler.

Expo instead shows a graceful degradation of accuracy for large real-time factors, making it an excellent candidate for fast low-accuracy simulations, which are typically desirable in MPC. In general, the *Expo* versions using a reduced number of mmm outperformed the standard *Expo*, but which number of mmm is optimal depends on the specific test and time step. As expected, when δt is smaller we can use a lower number of mmm. Finding an automatic way of choosing the optimal number of mmm is an interesting direction for future work.

B. Stiffness and Damping

This subsection investigates the sensitivity to contact stiffness and damping ratio. The damping ratio is defined as $\frac{B}{2\sqrt{K}}$. A damping ratio of 1 corresponds to a *critically damped* contact. These results are based on the “solo-trot”

¹<https://github.com/andreadelprete/consim>

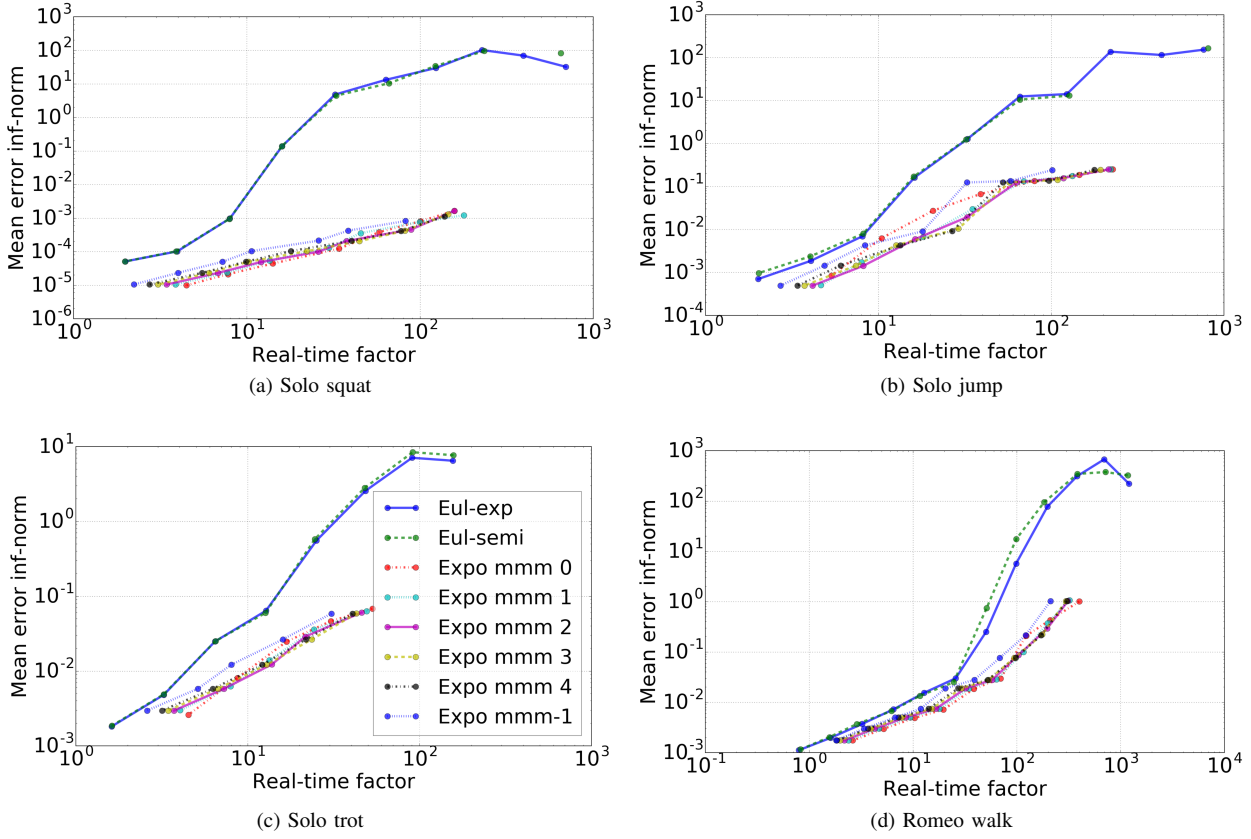


Fig. 2: Local integration errors vs real-time factors. The label *mmm-1* in the legend corresponds to using the default number of matrix-matrix multiplications in the computation of the matrix exponential.

scenario. For *Eul-exp* we have used $\delta t=1/8$ ms (real-time factor ≈ 12), which is the largest value giving a stable simulation for $K = 10^5$, $B = 10^2$. Then, we have set $\delta t=1/2$ ms for *Expo* so that it had roughly the same computation time.

Fig. 3 shows the local integration error as we vary the contact stiffness (with fixed damping ratio) and the damping ratio (with fixed contact stiffness). *Expo* shows a graceful degradation of performance as damping ratio and stiffness increase. The error of *Eul-exp* instead is highly affected by both stiffness and damping. In particular, *Eul-exp* performs well—almost as good as *Expo*—for $K = 10^4$, but it becomes quickly unstable as stiffness increases (we could not get any meaningful results for $K > 10^7$), and its performance also quickly deteriorates for lower stiffness values. *Expo* instead performs consistently up to $K = 10^8$, which roughly corresponds to a ground penetration of 0.01 mm for 100 Kg of weight on a single contact point. In terms of damping, *Eul-exp* performed worse as the damping increased. This is probably due to its inability to account for the variations of contact forces during the time step due to rapid changes in contact velocity occurring when the feet hit the ground.

C. Stability

To test the stability of the simulators we have repeated the previous tests, but without resetting the state to the

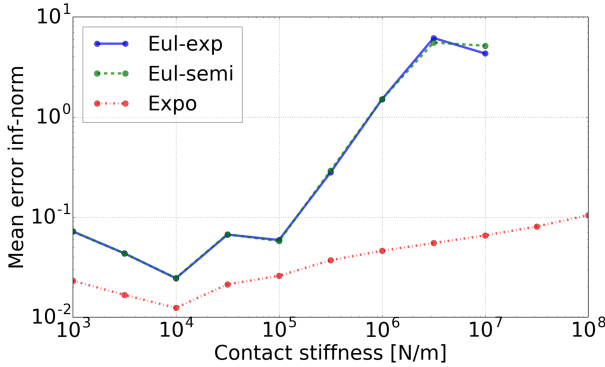
TABLE II: Maximum integration time steps to achieve a stable motion.

| Test | <i>Expo</i> δt [ms] | <i>Eul-exp</i> δt [ms] | <i>Eul-semi</i> δt [ms] |
|------------|-----------------------------|--------------------------------|---------------------------------|
| Solo-squat | 10 | $10/64 \approx 0.16$ | $10/64 \approx 0.16$ |
| Solo-jump | 10 | $10/8 = 1.25$ | $10/8 = 1.25$ |
| Solo-trot | 2 | $2/16 \approx 0.13$ | $2/16 \approx 0.13$ |
| Romeo-walk | $40/8 = 5$ | $40/32 = 1.25$ | $40/32 = 1.25$ |

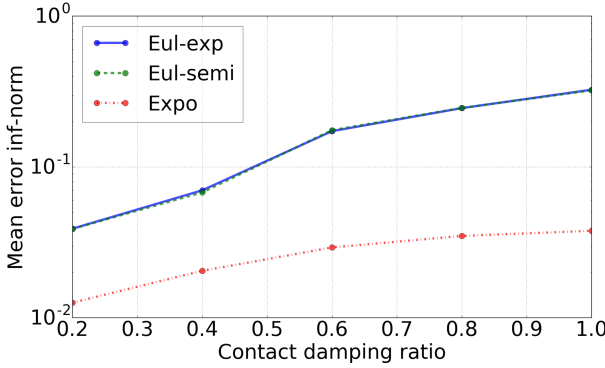
ground truth after every control loop. Table II reports, for each simulator, the largest integration time step for which the system remained stable. In three out of the four tests, *Expo* remained stable for the maximum time step that we could use, which was the controller time step. In the test “romeo-walk” *Expo* needed a smaller time step (5 ms) to remain stable. In all tests *Eul-exp* and *Eul-semi* performed very similarly, needing a time step between 4 and 64 times smaller than *Expo* to remain stable. The largest stable time step for Euler was 1.25 ms, whereas *Expo* reached 10 ms.

D. Force Prediction

To gain some insights into the internal computations of *Expo*, we show in Fig. 4 the contact forces predicted with (11) assuming constant A and b —which is the key assumption of our method. Since A and b depend on q and v , which vary during the time step, one could expect



(a) Varying contact stiffness (with fixed damping ratio of 0.5)



(b) Varying contact damping ratio (with fixed stiffness of 10^5 N/m).

Fig. 3: Local integration errors vs contact stiffness and damping ratio for the “solo trot” test using a fixed integration time step for *Eul-exp* (1/8 ms) and *Expo* (1/2 ms).

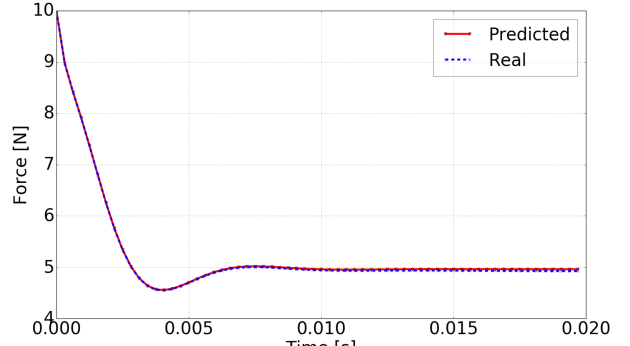
TABLE III: Computation times of *Expo* for “solo-trot”, using zero matrix-matrix multiplications for computing the matrix exponential (in parentheses the values corresponding to using the standard matrix exponential routine).

| Operation | Mean Time [μs] | Percentage of Total Time [%] |
|----------------------|----------------|------------------------------|
| step | 39 (94) | 100 |
| computeIntegrals | 13 (67) | 33 (72) |
| prepareExpLDS | 13 | 33 (14) |
| computeContactForces | 8 | 20 (8) |
| <i>Eul-exp</i> step | 9 | - |

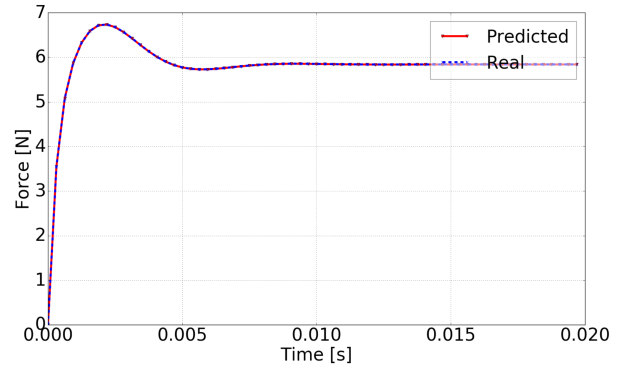
that neglecting their variations would result in significant force prediction errors. However, Fig. 4 shows that the force prediction can be accurate over a rather long time horizon (20 ms). These forces were generated at the beginning of the “solo-squat” test, using different initial velocities.

E. Computation Times

We report here a breakdown of the computation time of our method. The times shown in Tab. III are for the “solo-trot” test, which means that $v \in \mathbb{R}^{18}$ and most of the times $\lambda \in \mathbb{R}^6$. Most computation time (86%) is spent in three operations: `computeIntegrals`, `prepareExpLDS`, and `computeContactForces`. `computeIntegrals` boils down to computing a matrix exponential. This takes 72% of the total time when using a standard `expm` routine (without



(a) Contact velocity at impact: 0.1 m/s.



(b) Zero contact velocity at impact.

Fig. 4: Comparison of contact forces in normal direction with forces predicted using matrix exponential.

balancing and reduced matrix-matrix multiplications), but it goes down to 33% with our optimized version using zero matrix-matrix multiplications—we have seen in Fig. 2 that often this results in only a small loss of integration accuracy. The preparation of the linear dynamical system (11) (`prepareExpLDS`, which includes the computations of $h(q, v)$ with RNEA, $M(q)$ with CRBA, and Υ with a custom sparse Cholesky decomposition) takes an equal amount of time: 13 μ s on average, namely 33% of the total time. The third operation (`computeContactForces`) takes 20% of the total time, and it includes the computation of all kinematic quantities (contact point positions, velocities, accelerations, Jacobian) and the contact detection.

We believe that computation times could be improved, especially for the first two operations. In `computeIntegrals` we could test novel techniques [20] to compute the matrix exponential, exploit the sparse structure of the matrix A , and warm-start the computation using quantities computed at the previous cycle. In `prepareExpLDS`, the inverse contact-space inertia matrix Υ could be computed faster using a customized algorithm, rather than with products between J , M^{-1} and J^\top [31]. Overall, it seems impossible to reach the same efficiency of a simple *Eul-exp* step (9 μ s), but we think we could reach computation times in the range [20, 30] μ s.

VII. CONCLUSIONS

This paper has presented a new approach to simulate articulated systems subject to stiff visco-elastic frictional contacts. The novelty of the approach lies in the numerical integration, which applies a first-order Exponential Integrator scheme to the contact point dynamics to obtain a time-varying expression of the contact forces. These contact forces are then integrated analytically, exploiting theoretical results on the integrals of the matrix exponential [26], and advanced numerical algorithms for its fast computation [18]. Comparison with a standard explicit Euler scheme highlighted the benefits of the proposed approach in terms of speed-accuracy trade off, and stability.

Given its good behavior in the high-speed/low-accuracy regime, we believe that this simulation technique could be an excellent candidate for MPC. To do that, we will need to differentiate the integration scheme, which should be relatively easy given the simple analytical derivative of the matrix exponential. We are also interested in improving computational efficiency, working both on the computation of the needed dynamics quantities and the matrix exponential.

REFERENCES

- [1] M. Anitescu and G. D. Hart, “A constraint-stabilized time-stepping approach for rigid multibody dynamics with joints, contact and friction,” *International Journal for Numerical Methods in Engineering*, vol. 60, no. Jan 2003, pp. 2335–2371, 2004.
- [2] E. Todorov, “Implicit nonlinear complementarity: A new approach to contact dynamics,” in *2010 IEEE International Conference on Robotics and Automation*, no. 5. Ieee, may 2010, pp. 2322–2329. [Online]. Available: <http://ieeexplore.ieee.org/lpdocs/epic03/wrapper.htm?arnumber=5509739>
- [3] ——, “Convex and analytically-invertible dynamics with contacts and constraints: Theory and implementation in MuJoCo,” in *Proceedings - IEEE International Conference on Robotics and Automation*, 2014, pp. 6054–6061. [Online]. Available: <http://homes.cs.washington.edu/~todorov/papers/TodorovICRA14.pdf>
- [4] J. Hwangbo, J. Lee, and M. Hutter, “Per-Contact Iteration Method for Solving Contact Dynamics,” *IEEE Robotics and Automation Letters (RAL)*, vol. 3, no. 2, pp. 0–8, 2018.
- [5] E. Drumwright, “An Unconditionally Stable First-Order Constraint Solver for Multibody Systems,” *arXiv preprint arXiv:1905.10828*, 2019. [Online]. Available: <http://arxiv.org/abs/1905.10828>
- [6] Y. Tassa, T. Erez, and E. Todorov, “Synthesis and stabilization of complex behaviors through online trajectory optimization,” in *Intelligent Robots and Systems (IROS), IEEE/RSJ International Conference on*, 2012, pp. 4906–4913. [Online]. Available: <https://dada.cs.washington.edu/homes/todorov/papers/MPCGetUp.pdf>
- [7] N. Mansard, A. Del Prete, M. Geisert, S. Tonneau, and O. Stasse, “Using a Memory of Motion to Efficiently Warm-Start a Nonlinear Predictive Controller,” in *IEEE International Conference on Robotics and Automation*, 2018, pp. 2986–2993.
- [8] J. Viereck, J. Kozolinsky, A. Herzog, L. Righetti, and R. O. Aug, “Learning a Structured Neural Network Policy for a Hopping Task,” *IEEE Robotics and Automation Letters (RAL)*, vol. 3, no. 4, 2018.
- [9] R. Featherstone, *Rigid body dynamics algorithms*. Springer Berlin, 2008, vol. 49.
- [10] K. Yamane and Y. Nakamura, “Stable penalty-based model of frictional contacts,” *Proceedings - IEEE International Conference on Robotics and Automation*, vol. 2006, no. January, pp. 1904–1909, 2006.
- [11] U. M. Ascher and L. R. Petzold, *Computer methods for ordinary differential equations and differential-algebraic equations*. Siam, 1998.
- [12] M. Anitescu, “A Fixed Time-Step Approach for Multibody Dynamics with Contact and Friction,” in *IEEE International Conference on Intelligent Robots and Systems*, vol. 4, 2003, pp. 3725–3731.
- [13] T. Erez, Y. Tassa, and E. Todorov, “Simulation Tools for Model-Based Robotics: Comparison of Bullet, Havok, MuJoCo, ODE and PhysX,” in *International Conference on Robotics and Automation*, 2015. [Online]. Available: <http://thejns.org/doi/10.3171/PED/2008/1/2/138>
- [14] E. Drumwright and D. A. Shell, “Modeling contact friction and joint friction in dynamic robotic simulation using the principle of maximum dissipation,” in *Springer Tracts in Advanced Robotics*, vol. 68, no. STAR, 2010, pp. 249–266.
- [15] J. Loffeld and M. Tokman, “Comparative performance of exponential, implicit, and explicit integrators for stiff systems of ODEs,” *Journal of Computational and Applied Mathematics*, 2013.
- [16] J. Certaine, “The solution of ordinary differential equations with large time constants,” *Mathematical methods for digital computers*, vol. 1, pp. 128–132, 1960.
- [17] C. Moler and C. Van Loan, “Nineteen Dubious Ways to Compute the Exponential of a Matrix, Twenty-Five Years Later,” *SIAM Review*, vol. 45, no. 1, pp. 3–49, 2003. [Online]. Available: <http://epubs.siam.org/doi/10.1137/S00361445024180>
- [18] N. J. Higham, “The scaling and squaring method for the matrix exponential revisited,” *SIAM Journal on Matrix Analysis and Applications*, vol. 26, no. 4, 2005.
- [19] A. H. Al-Mohy and N. J. Higham, “Computing the Action of the Matrix Exponential, with an Application to Exponential Integrators,” *SIAM Journal of Scientific Computing*, vol. 33, no. 2, pp. 488–511, 2011.
- [20] J. Sastre, J. Ibáñez, and E. Defez, “Boosting the computation of the matrix exponential,” *Applied Mathematics and Computation*, vol. 340, no. August, pp. 206–220, 2019.
- [21] D. L. Michels, G. A. Sobottka, and A. G. Weber, “Exponential integrators for stiff elastodynamic problems,” *ACM Transactions on Graphics*, vol. 33, no. 1, 2014.
- [22] Y. J. Chen, U. M. Ascher, and D. K. Pai, “Exponential Rosenbrock-Euler Integrators for Elastodynamic Simulation,” *IEEE Transactions on Visualization and Computer Graphics*, vol. 24, no. 10, pp. 2702–2713, 2018.
- [23] V. T. Luan and D. L. Michels, “Explicit Exponential Rosenbrock Methods and their Application in Visual Computing,” *arXiv preprint arXiv:1805.08337*, pp. 1–18, 2018. [Online]. Available: <http://arxiv.org/abs/1805.08337>
- [24] E. Todorov, T. Erez, and Y. Tassa, “MuJoCo: A physics engine for model-based control,” in *Intelligent Robots and Systems (IROS), IEEE/RSJ International Conference on*, 2012. [Online]. Available: https://dada.cs.washington.edu/homes/todorov/papers/MuJoCo.pdfhttp://ieeexplore.ieee.org/xpls/abs_-all.jsp?arnumber=6386109
- [25] C. F. Van Loan, “Computing Integrals Involving the Matrix Exponential,” *IEEE Transactions on Automatic Control*, vol. 23, no. 3, pp. 395–404, 1978.
- [26] F. Carbonell, J. C. Jímenez, and L. M. Pedroso, “Computing multiple integrals involving matrix exponentials,” *Journal of Computational and Applied Mathematics*, vol. 213, no. 1, pp. 300–305, 2008.
- [27] A. H. Al-Mohy and N. J. Higham, “A New Scaling and Squaring Algorithm for the Matrix Exponential,” *SIAM Journal on Matrix Analysis and Applications*, vol. 31, no. 3, 2010.
- [28] F. Grimmerger, A. Meduri, M. Khadiv, J. Viereck, M. Wuthrich, M. Naveau, V. Berenz, S. Heim, F. Widmaier, T. Flayols, J. Fiene, A. Badri-Spowitz, and L. Righetti, “An Open Torque-Controlled Modular Robot Architecture for Legged Locomotion Research,” *IEEE Robotics and Automation Letters*, vol. 5, no. 2, pp. 3650–3657, 2020.
- [29] “Project Romeo <http://projetromeo.com>.”
- [30] J. Carpentier, G. Saurel, G. Buondonno, J. Mirabel, F. Lamiriaux, O. Stasse, and N. Mansard, “The Pinocchio C++ library: A fast and flexible implementation of rigid body dynamics algorithms and their analytical derivatives,” *Proceedings of the 2019 IEEE/SICE International Symposium on System Integration, SII 2019*, pp. 614–619, 2019.
- [31] R. Featherstone, “Exploiting sparsity in operational-space dynamics,” *The International Journal of Robotics Research*, vol. 29, no. 10, pp. 1–21, 2010. [Online]. Available: <http://ijr.sagepub.com/content/29/10/1353.short>